Synthesis of bioactive class II poly(γ-glutamic acid)/silica hybrids for bone regeneration

Gowsihan Poologasundarampillai,[a] Claudia Ionescu,[b] Olga Tsigkou,[a,c] Muthu Murugesan,[d] Robert G Hill,[e] Molly M Stevens,[a,c] John V Hanna[b], Mark E Smith[b] and Julian R Jones*[a]

Received (in XXX, XXX) Xth XXXXXXXXX 200X, Accepted Xth XXXXXXXXX 200X
First published on the web Xth XXXXXXXXX 200X
DOI: 10.1039/b000000x

Abstract

Bone grafts are commonly used to regenerate bone in defect sites resulting from disease or trauma but there is clinical need for artificial materials that will be readily available and reduce pain and recovery time for the patient. Current artificial bone graft materials are bioactive ceramics and glasses, which are too brittle for bone defects that experience cyclic load. The synthesis of a new nanocomposite material is described that has the potential of being a tough off-the-shelf artificial bone graft that can regenerate a bone defect and have enough flexibility to press-fit into place. The poly(γ-glutamic acid)/bioactive silica hybrid material with composition 40 wt% organic and 60 wt% bioactive inorganic (composition 70 mol% SiO_2 and 30 mol% CaO) was synthesised using a sol-gel route. The potential advantage of a hybrid material over conventional composites is the molecular scale interactions between the bioactive inorganic and the tough degradable organic. The organic and inorganic chains were covalently cross-linked using an organosilane that has an organic functionality to bond to poly(γ-glutamic acid) (γ-PGA) and an alkoxysilane group that condenses with the inorganic phase. The covalent cross-linking (class II hybrid)is required to control the dissolution and improve mechanical properties of the material. The two key variables, the concentration of cross-linking agent and the addition of calcium, were investigated by ^{29}Si solid-state NMR and electron microscopy. The hybrid materials were bioactive in simulated body fluid (SBF) with a hydroxy carbonate apatite (HCA) layer detected after immersion for 72 h. The hybrid material favours cell attachment and is not cytotoxic as demonstrated by culture of the osteosarcoma cell line SaOs-2 on the material for 4 days.

Introduction

Bone grafts

Autografts (bone grafted from the patient) and allografts (bone from a bone bank) are used for treating the majority of bone defects.[1] Autografts are the most popular choice due to their osteoconductive (ability of a material in contact with host bone to form a strong bond to it and enable the bone to grow along it) and osteoinductive (ability of a material to recruit osteoprogenitor cells and signal them to divide into osetoblasts which lay down new bone away from a bone site) properties, but they are limited in supply and the harvest also give rise to donor site pain and morbidity.[2, 3] Allografts are plentiful, however they are treated to remove cells and proteins that could potentially transmit disease and therefore lose their osteogenic properties and have low strength. Synthetic bone grafts (also called alloplasts) such as hydroxyapatite, Bioglass®[4] and tricalcium posphates[2] are also currently used, but are brittle, their degradation rate is difficult to tailor and clinicians cannot easily cut them to shape. Therefore a real need exists for a new synthetic bone graft material that better matches the properties of bone.[5]

Synthetic bone graft substitutes

An optimum synthetic bone graft substitute should fulfil several criteria: it should:[6-8]

1 resorb at the same rate as the bone forms,
2 be biocompatible and products of resorption should not be toxic,
3 be osteoconductive and osteogenic,
4 exhibit mechanical properties similar to the host trabecular bone,
5 act as a template for three-dimensional bone tissue growth with interconnected macroporous network.

Synthetic constructs for bone regeneration have been made from inorganic and organic materials.[9-11] One example of an inorganic construct for bone regeneration is the sol-gel derived bioactive glasses.[7] Jones *et al.* developed macroporous bioactive glass foams that can form an HCA layer after 72 h of immersion in SBF. The same foams where also shown to have a compressive strength of σ_{max} = 2.3 MPa, which is in the compressive strength range of human trabecular bone.[7] However they were brittle owing to their glassy nature. Organic constructs can be made of resorbable polyesters, such as the poly(lactic co-glycolic acid) (PLGA) foams.[12] Polymeric foams are extremely tough and flexible, however they are not inherently bioactive and are weak in compression, therefore they do not fulfil all the required criteria.[13]

Composites of inorganic and organic components are a promising way forward in overcomming the lack of toughness in inorganic materials and lack of strength in organic materials.[14-17] Poly(lactic acid)/ tricalcium phosphate particle composites produced by Xiong *et al.* using the low-temperature deposition manufacturing method are an example of a composite containing biodegradable polymer and a bioactive phase.[16] In this material a compressive strength of 4.71 MPa for a scaffold with 89% porosity was achieved. However, in conventional composites which have macro-scale phase domains, the dissolution rate can often be unpredictable, leading to rapid loss of mechanical properties.

Bone is a composite at the nano-scale of mineral hydroxyapatite and organic collagen, a structure which contributes its excellent mechanical properties. Reports have been published that show that the nanosized bioactive particles have better apatite forming ability than macrosized particles.[18, 19] Therefore a composite with nanosized inorganic/organic domains may have improved bioactivity.[20-22]An additional advantage is that nanocomposties will provide greater control over degradation.

Hybrid material for bone graft

The surface-to-volume ratio and interfacial area between the two phases play a large role in the dissolution rate and mechanical properties of a hybrid material. Sol-gel hybrids are known to have high surface-to-volume ratio which allows for the production of advanced materials with improved control and tunable properties.[23, 24]

The low-temperature production of inorganic materials utilising the versatile sol-gel technique has been adopted to produce inorganic/organic hybrid materials, resulting in materials with high surface-to-volume ratio and nano-scale phase domains.[25-30] The molecular interaction in the sol and the bonding between the two phases often determine the final properties of the material.[31] Their interaction can be controlled by the use of surfactants and solvents, while the bonding can be altered to range from weak forces (Van der Waals', hydrogen and ionic bonding between the inorganic and organic, where the material is defined as a class I hybrid) to strong covalent bonds (class II) by the use of coupling agents such as organosilanes.[32] The surfactants and solvents function to stabilise the steric forces and allow dispersion of the two phases.[33] Organosilanes are molecules that have organic and inorganic functional moieties in the same molecule which can bond to organic and inorganic chains, respectively. Ren *et al.* used this concept to produce a class II biodegradable gelatin-siloxane hybrid by covalently crosslinking gelatin with the organosilane glycidoxypropyl trimethoxysilane (GPTMS).[34] However, the inorganic loading in the hybrids was much too low to give high compressive strength.

The selection of the correct organic phase is extremely important, it must be compatible with the sol-gel process and have functional groups to react with the organosilanes. The

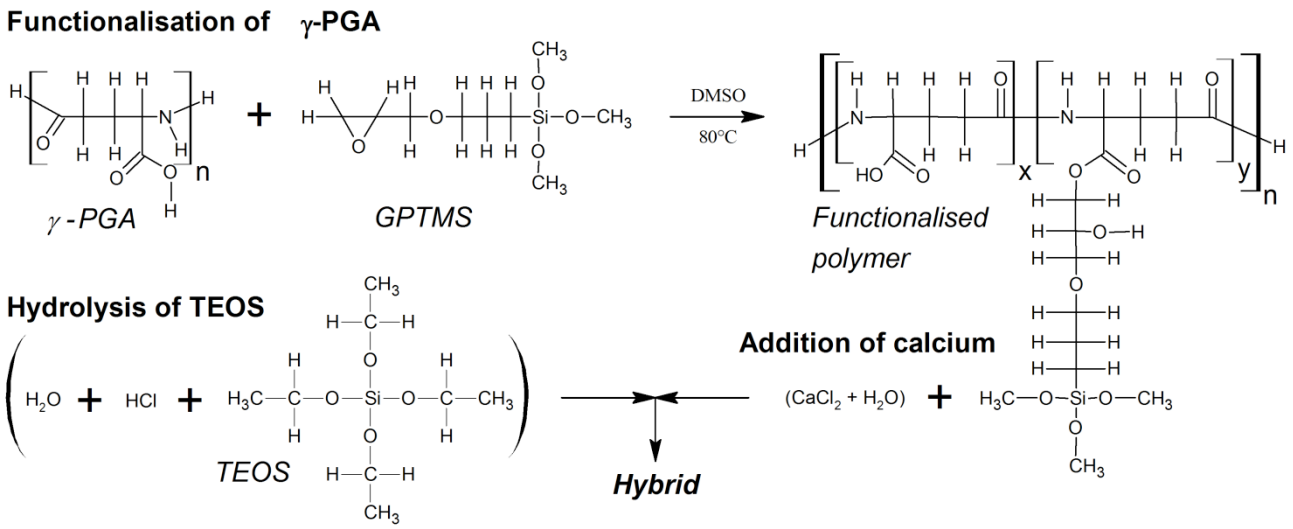

Fig. 1 Schematic of the two pot reaction for the hybrid synthesis. Poly(γ-glutamic acid) and glycidoxypropyl trimethoxysilane (GPTMS) are first reacted to get silane coupling on the polymer. Then calcium is added as $CaCl_2$ dissolved in water. In the second pot the TEOS is hydrolysed in acidic conditions. The two pots are mixed together resulting in the hybrid precursor sol.

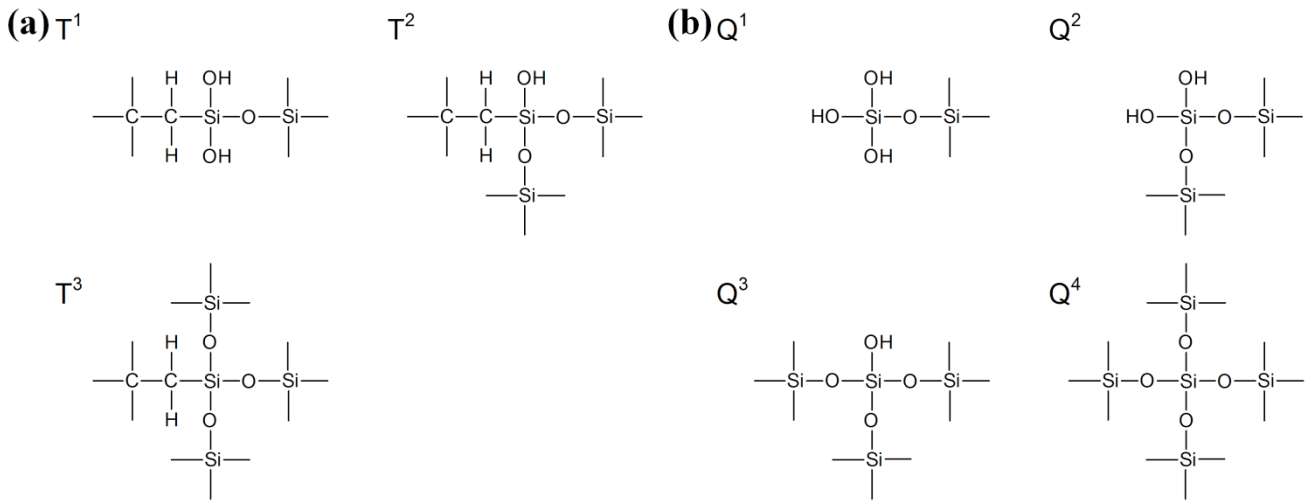

Fig. 2 The T^n and Q^n Si-O bridging configurations that could occur in the hybrid material as determined by ^{29}Si NMR.

bacterially synthesised γ-PGA (chemical structure shown in Fig. 1) is a little known polymer in the field of tissue engineering.[35, 36] Reports have indicated that sequences of glutamic acid residues are found in bone at the end of collagen fibrils and that they have a role in HCA nucleation.[37, 38] This property of γ-PGA has been successsfully utilised to fabricate γ-PGA/HCA composites by the immersion of the polymer in a solution containing calcium and phosphate.[36] γ-PGA is biodegradable and has a reactive carboxylic acid on its side group which allows for functionalisation. For regenerating bone, γ-PGA is an alternative to polyesters such as PLA or PGA that degrade by hydrolysis (random chain scission), which can cause rapid loss of mechanical properties once degradation begins. In contrast γ-PGA degrades enzymatically from the surface.

In this article the synthesis and the characterisation of a hybrid that has the potential to fulfil the criteria for bone regeneration listed above is presented.

Results and Discussion

Synthesis of a hybrid containing γ-PGA and calcium

Fig. 1 shows the reaction schematic of the two-pot hybrid synthesis. γ-PGA was first functionalised with the organosilane GPTMS, where the carboxylic acid of the polymer was reacted with the epoxy group on the GPTMS by ring opening esterification. During the functionalisation process it was found that the inorganic functional group trimethoxysilane on GPTMS had hydrolysed and partially condensed to other GPTMS molecules forming Si-O-Si bridging oxygens. Using ^{29}Si solid-state magic angle spinning

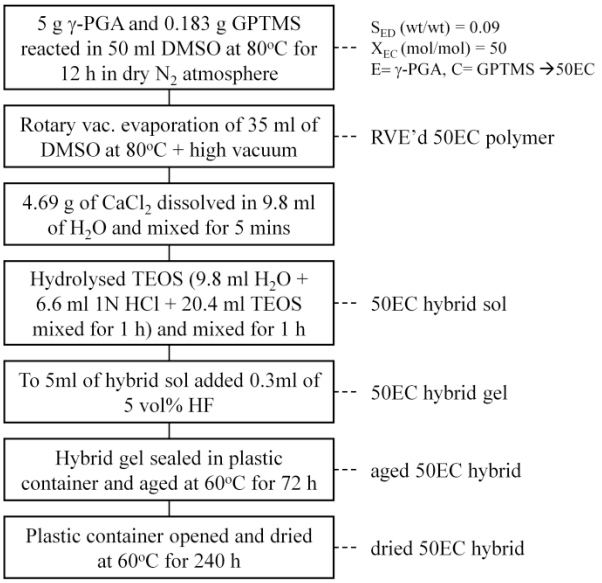

Fig. 3 Flow chart showing the reaction and processing steps involved in the synthesis of the hybrid material.

Table 1 Summary of the influence of the three processing parameters during coupling reaction on the condensation of the GPTMS trimethoxy silicate groups.

Reaction condition varied			Influence on degree of condensation (D_C)	
S_{ED} (γ-PGA:DMSO) ratio	0.03→0.06	(x2)	90.8 → 79.4 %	(x 0.87)
X_{EC} (γ-PGA:GPTMS) ratio	2.00→5.00	(x2.5)	41.1 → 76.6 %	(x 1.86)
Reaction time (h)	4→8	(x2)	41.1 → 68.5 %	(x 1.7)

(MAS) NMR it was possible to quantify the proportion of condensed and free silicate species. Fig. 2 shows the T and Q silica condensation states that are possible in the hybrid. The T^n network have n = 0, 1, 2 and 3, and Q^n network have n = 0, 1, 2, 3 and 4, with T^0 and Q^0 representing no condensation and T^3 and Q^4 maximum condensation.

Table 1 shows the influence of the reaction conditions on the degree of condensation (D_c), where D_c is a measure of the extent of condensation and is given by equation 1.

$$D_c = \left(\frac{1T^1 + 2T^2 + 3T^3}{3}\right) \times 100\% \qquad (1)$$

Increasing the solute (γ-PGA) concentration, γ-PGA:DMSO ratio (S_{ED}), caused D_c to decrease. E.g. doubling the amount of polymer while keeping the amount of DMSO constant (γ-PGA:GPTMS ratio was also kept constant) was found to decrease D_c from 90.8 % to 79.4%. This reduction in condensation of silicate species was attributed to the increased competition for the dissolved water for hydrolysis in the reaction mixture and the steric hindrance of the motion of the GPTMS molecules as solute concentration increased. The influence of the γ-PGA:GPTMS ratio (X_{EC}) and the reaction time on the condensation of GPTMS were also studied. D_c was found to increase as both parameters increased. The X_{EC} ratio indicates the extent of organic and inorganic crosslinking in the hybrid, the higher the ratio the lower the crosslinking. Surprisingly, decreasing the concentration of GPTMS resulted in an increase in D_c, where the contrary was expected. Although the concentration of species for potential condensation increased, the amount of water remained constant therefore there was significant competition for water from the increased GPTMS and hence only partial condensation was possible. Doubling the reaction time increased D_c by a factor of 1.7, as a result of increased time for the molecules to move around and condense. Fig. 3 shows

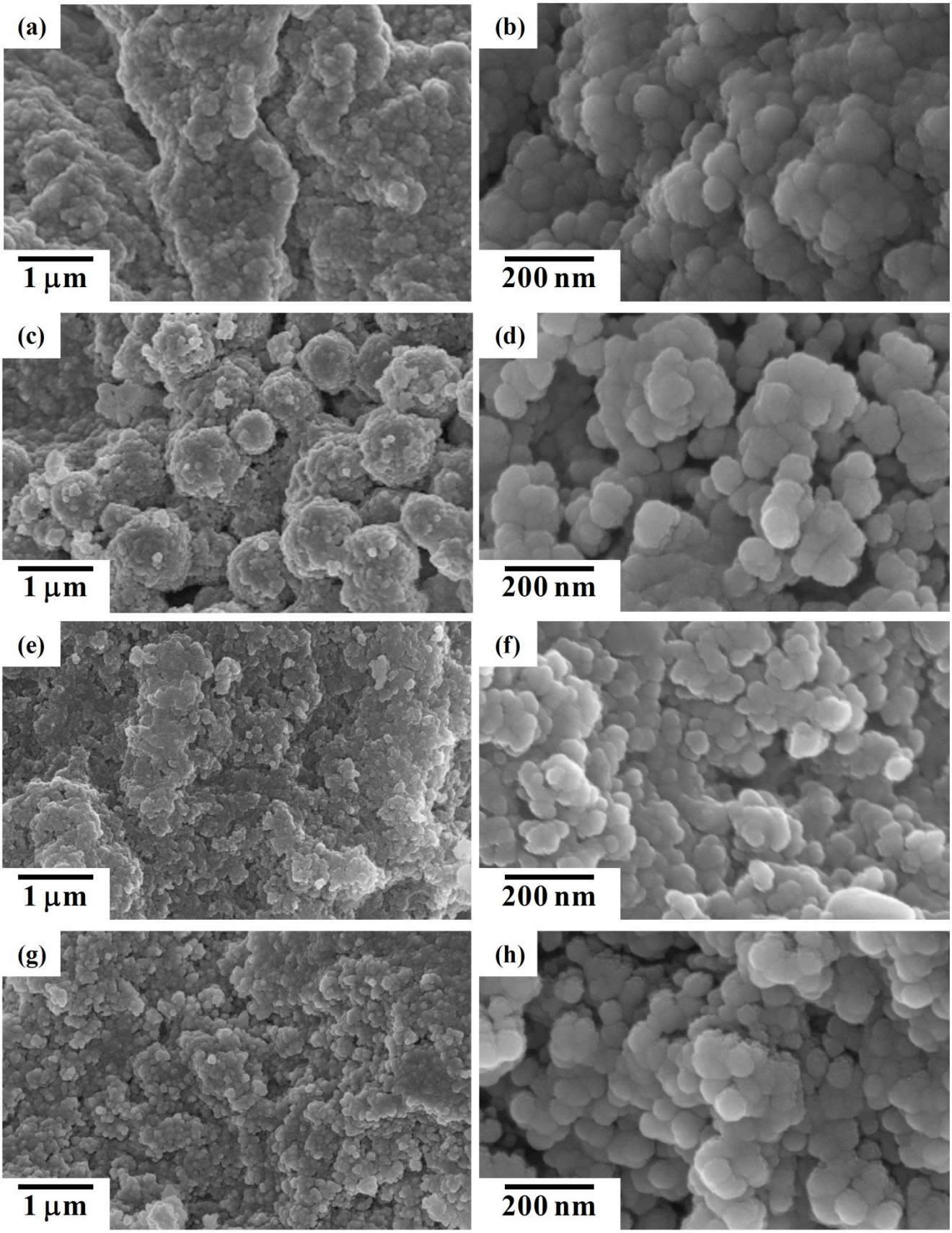

Fig. 4 SEM images of the fracture surface of hybrids containing 40 wt% organic, 60 wt% inorganic and γ-PGA:DMSO ratio (S_{ED}) of 0.09 (a,b), 0.23 (c,d), 0.26 (e,f) and 0.45 (g,h).

the S_{ED} ratio and the reaction time chosen for the polymer to GPTMS coupling.

The second step in the synthesis of the hybrid was the addition of calcium chloride solution to the functionalised polymer (Fig. 1). The inorganic sol was prepared by the hydrolysis of the silica precursor tetraethyl orthosilicate (TEOS) in acidic conditions in a separate beaker. The two solutions were added together to create the hybrid sol (Fig. 1). The hybrid sol was poured into polymethyl propylene moulds and gelled by hydrofluoric acid (HF). The gelled hybrids were sealed and aged at 60°C and dried at 60°C. The flow diagram in Fig. 3 summarises the synthesis of a hybrid with 60/40 wt% inorganic/organic constituents and glutamic acid:GPTMS ratio of 50 containing calcium termed 50ECCa (E = glutamic acid, C = GPTMS and Ca = calcium).

Influence of DMSO on nanostructure

The amount of DMSO solvent had a large effect on the gelation rate and the resulting nanostructure and nanoporosity. Fig. 4 shows the SEM images of the fracture surface of hybrids of 40 wt% functionalised γ-PGA, 60 wt% SiO_2 (no calcium) gelled with HF. The samples were prepared with X_{EC} and S_{ED} ratios of 50 and 0.09 respectively. Importantly, for three of the hybrid samples in Fig. 4 large amounts of DMSO were removed by evaporation after the γ-PGA to GPTMS coupling reaction to study the influence of DMSO content on the hybrid, resulting in samples with S_{ED} ratio of 0.23, 0.26 and 0.45. The presence of DMSO in the hybrid sol was found to have a large influence on the silicate condensation reaction. By reducing the DMSO present in the hybrid sol from an S_{ED} ratio of 0.09 to 0.45 the gelling time with HF reduced from 25 days to ~6 minutes. The micro and nano structures of the hybrid samples with S_{ED} ratio of 0.09 (Fig. 4a & b), 0.23 (Fig. 4c & d), 0.26 (Fig. 4e & f) and 0.45 (Fig. 4g & h) are shown in Fig. 4. The nanostrucutre of all the samples were composed of 50–100 nm sized particles, similar to the morphology observed for sol-gel glasses observed by Lin *et al.*[39], who followed the formation of nanoparticles in the sol-gel bioactive glasses using electron microscopy and ^{29}Si NMR. They showed that hydrolysis and condensation of TEOS results in primary particles of silica which aggregate to form colloidal particles (called secondary particles) with diameters of approximately 5 nm in the sol. The further polycondensation and aggregation of silica secondary particles leads to gelling of the solution. Ageing and drying the gel at low temperature promotes more condensation and the secondary particles coalesce to form the tertiary particles which are of the order of 10–30 nm. The particles in Fig. 4 were larger than found by Lin *et al.*, this was because the hybrid was gelled with HF which is a stronger catalyst than the nitric acid used by Lin *et al.* The HF accelerates condensation by providing low-energy sites and hence larger particles were produced.[40] The micro-scale morphology of the samples show a homogeneous packing of the nanoparticles, except in the hybrid sample with an S_{ED} ratio of 0.23 where larger particles of ~1 μm composed of the nanoparticles were found. The SEM images (Fig. 4a, c, e, g)

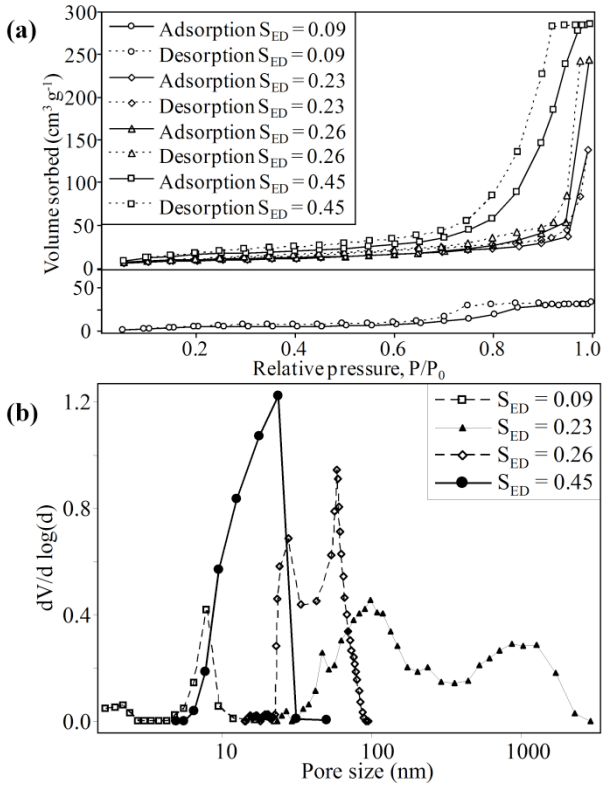

Fig. 5 (a) Nitrogen sorption isotherms of hybrids with various γ-PGA:DMSO ratios (S_{ED}) and (b) pore size distributions of the same materials obtained from the N_2 desorption isotherm and mercury porosimetry.

Table 2 Summary of the meso and macro porosity of the hybrids with γ-PGA:DMSO ratio (S_{ED}) of 0.09, 0.23, 0.26 and 0.45.

S_{ED} Ratio	Surface area (m^2/g)	pore size (nm)	Pore volume (cm^3/g)	BET Constant C
0.09	28.6	7.80	0.052	6.50
0.23	33.0	[a]98.5, 1040	[a]0.441	27.9
0.26	37.5	[a]27.6, 58.1	[a]0.265	35.3
0.45	64.3	23.6	0.443	19.0

[a] Data obtained from mercury porosimetry measurements.

show that the particles were more closely packed in the sample containing the most DMSO (S_{ED} ratio = 0.09).

Nitrogen sorption and mercury porosimetry were performed on the calcium-free hybrid samples to quantify the influence of DMSO removal on the pore network. Fig. 5a shows the isotherms obtained from N_2 sorption.[41] The shape of the isotherms (Type IV) of hybrids with S_{ED} ratios of 0.09 and 0.45 indicated that the materials were mesoporous. The hysteresis loops suggest interconnected mesopores with interconnects between the pores having smaller diameter than the maximum pore diameter. The adsorption increased as S_{ED} increased, indicating increasing surface area of adsorption. Table 2 shows the surface area, pore size and total pore volume of the four samples. The surface area of the hybrids increased as the DMSO content decreased; e.g. the hybrid with the lowest DMSO content (S_{ED} ratio of 0.45) had the highest surface area of 64.3 m^2g^{-1}. This indicates that higher concentration of DMSO induced densification of the hybrids.

Fig. 5b shows the pore size distributions obtained from N_2 sorption (for S_{ED} 0.09 and 0.45) and mercury porosimetry (for S_{ED} 0.23 and 0.26) for the four hybrid samples. Two different techniques were needed due to the different ranges of pore sizes. Hybrids with S_{ED} ratios of 0.09 and 0.45 were found to have pores in the mesopore range (2 – 50 nm) while the S_{ED} 0.23 samples had bimodal macropores (> 50 nm) and that with an S_{ED} of 0.26 contained both mesopores and macropores. The sample containing the maximum amount of DMSO (S_{ED} = 0.09) had the smallest modal pore size of 7.8 nm and the

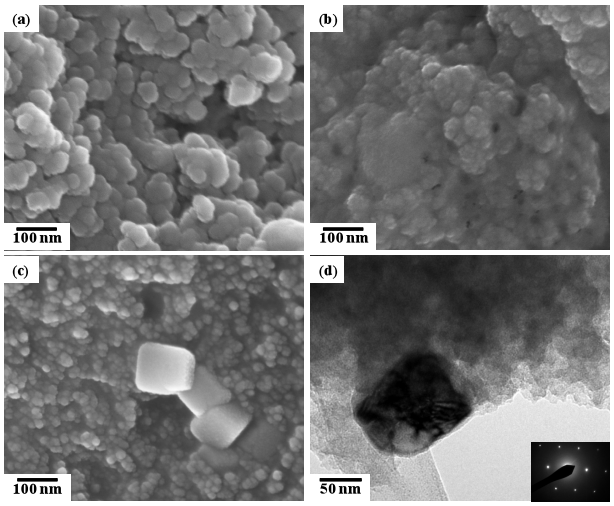

Fig. 6 SEM and TEM images showing the influence of calcium on the nanostructure of the hybrids. SEM image of hybrid without calcium (a), with calcium (b,c) and TEM image of hybrid with calcium (d).

lowest pore volume. This is confirmed by the SEM images (Fig. 4a & b). The hybrid with an S_{ED} of 0.23 had a large pore volume (Table 2) compared to the samples with S_{ED} 0.09 and 0.26, also evident in the SEM images. Further, the BET constants C in Table 2 for the samples were lower than that of the sol-gel silica when N_2 was used as the absorbate ($50 < C < 200$).[42] This indicates that the surfaces of the hybrids were mainly covered with the polymeric phase.

Therefore it seems that for a γ-PGA/ silica hybrid to gel with HF at short times and have a continuous pore network it must have S_{ED} ratio higher than 0.23.

Influence of calcium on hybrid nanostructure

The incorporation of calcium ions into the hybrid is extremely important as it greatly influences the formation of an HCA layer and together with soluble silica, it stimulates the genes in the bone cells to increased differentiation and proliferation.[43] The samples containing calcium were transparent and yellowish, but the calcium-free samples were opaque. This was due to the presence of pores in the calcium-free hybrids. No pores were observed in the calcium-containing samples by nitrogen sorption or mercury porosimetry. Fig. 6a shows the SEM image of a hybrid without any calcium added and an S_{ED} ratio of 0.26. The morphology was similar to the particle-like morphology seen in Fig. 4. Fig. 6b shows the SEM image of a hybrid with same DMSO concentration and processing conditions as Fig. 6a but with calcium present; the nanostructure was very different. In the calcium containing hybrid the particles were smaller (<25 nm) and the porosity seen in the calcium-free hybrids were no longer visible, rather the pores were seen to be filled with the polymer. Fig. 6c and Fig. 6d show SEM and TEM images of a calcium-containing hybrid where the calcium has precipitated out as a nano crystalline phase identified by electron diffraction image (Fig. 6c insert). Although this was a rare occurence in the hybrid samples, it suggests that improved calcium sources or processing methods are needed for completely incorporating calcium into the hybrids at low

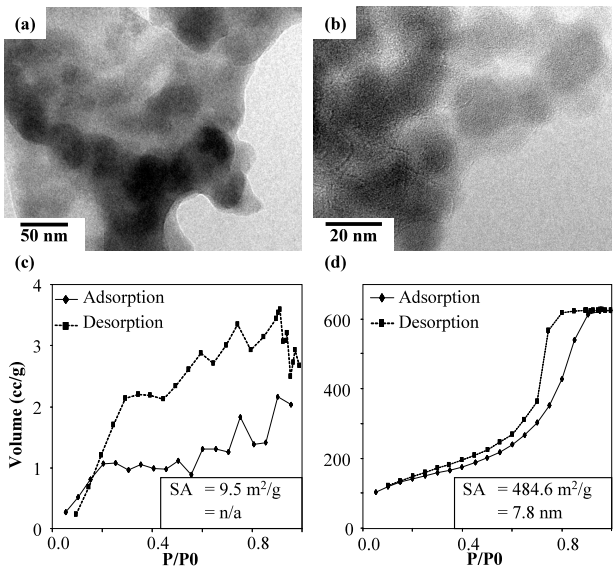

Fig. 7 TEM image and N_2 sorption isotherm of the hybrid before (a,c) and after extraction of the polymer (b,d).

temperature.

TEM images revealed that the silica nanoparticles formed an interconnected network throughout the material. Fig. 7a shows the TEM image of a 50ECCa hybrid with an S_{ED} ratio of 0.26. The curved edges and waves of dark and light contrast in the TEM image indicate particles of higher atomic mass embedded in a lower atomic mass material. This suggests that the particles are silica and that the matrix is composed of organic polymer. Fig. 7b shows the hybrid after the extraction of the polymer by complete dissolution, here the particles seem to be directly bonded to one another, leaving voids in their interstitial spaces. This indicates that the nanostructure is one where it consists of silica particles bonded together, with organic polymer filling the voids. N_2 sorption isotherms for the hybrid containing the polymer and with the polymer removed are shown in Fig. 7c & Fig. 7d respectively. Fig. 7c shows a negligible amount of adsorption meaning that the hybrid does not have any mesopores. However, once the polymer was extracted a large volume of N_2 was adsorbed. The isotherm of the sample after the extraction of the polymer was that of a Type IV indicating that the sample contains interconnected mesopores.[41] This supports the suggestion that the polymer was filling the mesopores in a continuous silica network within the hybrid. However, due to the open-ended nature of the mesopores the

polymer was also a continuous phase in the hybrid and therefore also behaves as a matrix. The surface area for hybrids with and without polymer were calculated using a BET model from the N_2 adsorption to be 9.5 and 484.6 m^2g^{-1}, respectively. The high surface area of the latter indicates a large interaction between the organic and inorganic when the polymer was present. The modal pore size was calculated to be 7.8 nm using the BJH model, since when polymer is present it fills this space it can be concluded that the polymer exhibits a minimum domain size of 7.8 nm. Therefore, the SEM, TEM and N_2 sorption show that the 50ECCa was a true hybrid, where both organic and inorganic phases play the role of a matrix from the lowest domain size of 25 nm up to the macroscale. This is good for the mechanical and dissolution properties of the hybrid. There is also the possibility that when cells contact the surface of the material they will interact with the surface as one continuous material rather than two separate phases.

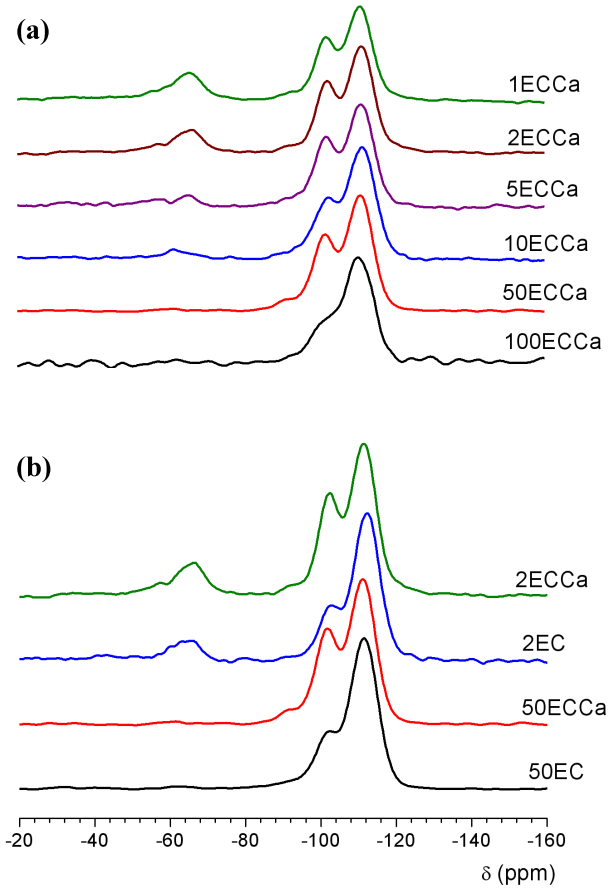

Fig. 8 ^{29}Si MAS NMR spectra of hybrids with increasing amounts of crosslinker (a) and with and without calcium (b).

Table 3 Chemical shifts and relative proportions of T^n and Q^n species in the hybrids with different proportions of coupling and with and without calcium.

Sample	T^1		T^2		T^3		Q^2		Q^3		Q^4	
	$^a\delta$ (ppm)	^bI (%)	$^a\delta$ (ppm)	^bI (%)	$^a\delta$ (ppm)	^bI (%)	$^a\delta$ (ppm)	^bI (%)	$^a\delta$ (ppm)	^bI (%)	$^a\delta$ (ppm)	^bI (%)
100ECCa	-	-	-	-	–62.3	2	–92.5	2	–101.4	25	–111.0	71
50ECCa	-	-	-	-	–61.1	1	–92.1	6	–101.5	33	–111.1	60
50EC	-	-	–60.7	1	–65.3	1	–92.3	4	–101.7	23	–111.5	71
10ECCa	-	-	-	-	–65.5	2	–93.6	5	–102.1	29	–111.6	62
					–61.1	2						
5ECCa	-	-	–57.4	3	–65.2	4	–94.4	4	–101.8	31	–111.2	58
2ECCa	–52.7	1	–57.1	2	–65.6	12	–93.0	4	–102.0	28	–111.4	53
2EC	-	-	–59.2	2	–65.0	9	–92.6	1	–102.5	22	–112.3	66
1ECCa	-	-	–56.4	5	–65.6	16	–92.9	4	–101.7	26	–111.0	49

$^a\delta$ and ^bI represent the ^{29}Si chemical shift and relative intensity, respectively. Errors associated with measurements are δ ± 2 ppm and Integral ±2%.

Influence of crosslinking on hybrid structure

Solid state ^{29}Si NMR was performed on the hybrid samples to first check the bonding of functionalised polymer to the inorganic network in the hybrid and secondly to quantify the proportions of the condensed silicate species. Fig. 8a shows the ^{29}Si MAS NMR spectra of 1ECCa, 2ECCa, 5ECCa, 10ECCa, 50ECCa and 100ECCa hybrids.

All the samples had both T^n and Q^n species (T^n and Q^n corresponds to the structures of $CSi(OSi)_n(OR)_{3-n}$ and $Si(OSi)_n(OR)_{4-n}$, respectively, where R is H, CH_3CH_2 or O^-, i.e. a non-bridging oxygen).[44] To quantify the Q^n distribution the ^{29}Si MAS NMR spectra were deconvolved by Gaussian fitting using DMFIT software.[45] The results of the Gaussian

fitting of all of the ^{29}Si MAS NMR spectra are summarised in Table 3.

In all samples the silica matrix condensed well, forming Si-O-Si bonds as shown by the dominance of Q^4 species in the hybrids. This is due to the influence of HF as a catalyst in the gelling process when highly branched clusters are obtained. [46] The proportion of T^n species, particularly the T^3, were found to decrease with increasing X_{EC} ratio. This shows that the GPTMS was successfully condensed in the hybrid and that with increased GPTMS a higher degree of inorganic/organic crosslinking was taking place. The proportion of Q^4 was found to increase with increasing X_{EC} (decreasing T^n), while the Q^3/Q^4 ratio was generally observed to decrease. This suggests that with higher concentration of GPTMS the silica particles were smaller and therefore more Q^3 species were present. This indicates that the increase in crosslinking decreased the silica particle size and increased inorganic/organic interaction.

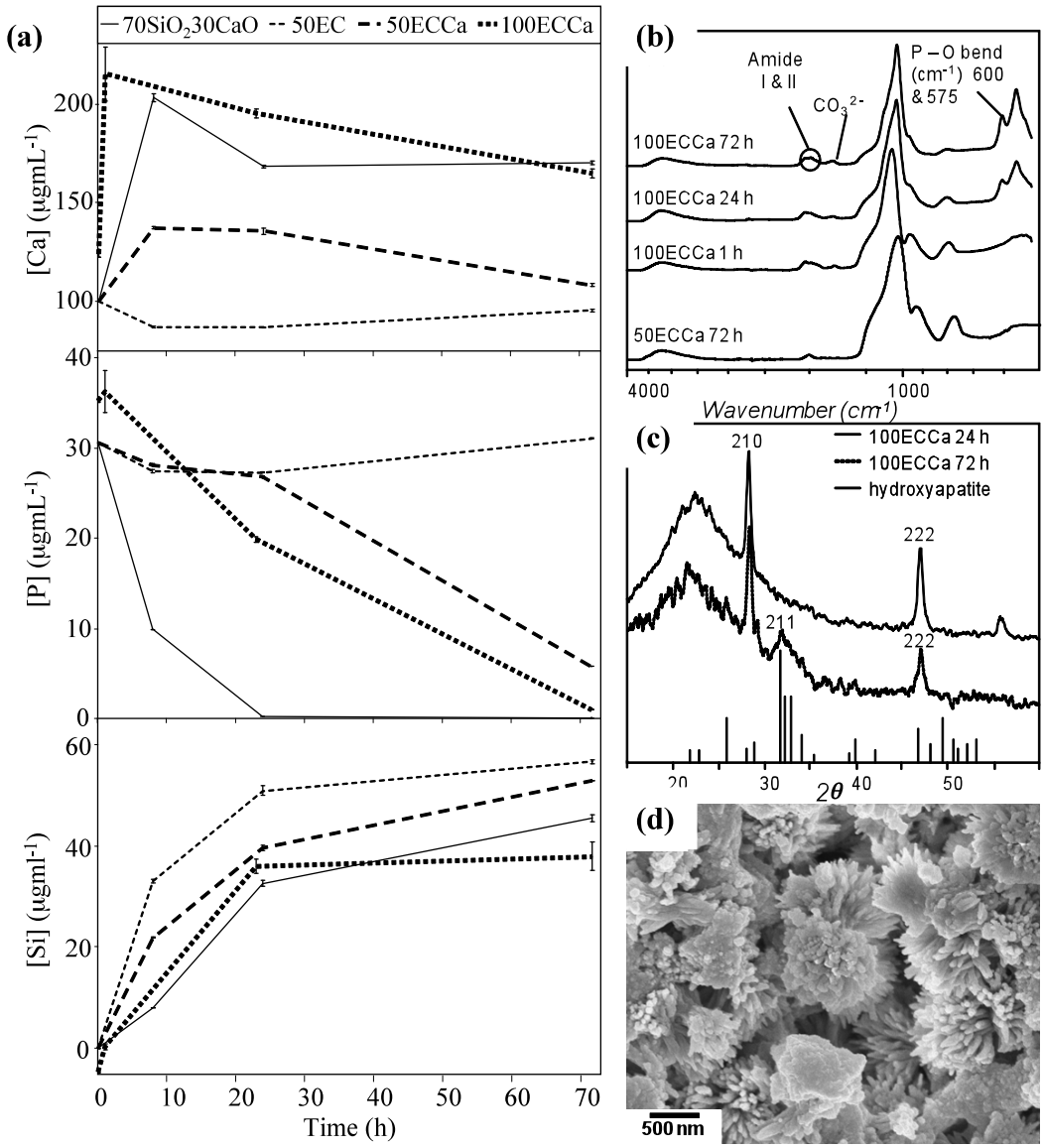

Fig. 9 SBF testing of $70SiO_2 30CaO$, 50EC, 50ECCa and 100ECCa. (a) ICP spectra of the SBF solutions removed at 1, 24 and 72 h. (b) FTIR spectra of 100ECCa after 1, 24 and 72 h soaking and of 72 h of soaked 50ECCa. (c) XRD spectra of 100ECCa hybrid sample after 24 and 72 h of soaking and of synthetic HCA (Reference code 00-009-0432). (d) SEM image of the 100ECCa sample after soaking for 72 h showing the needle like HCA particles formed on the hybrid.

Fig. 8b shows the ^{29}Si MAS NMR spectra of the 2ECCa and 50ECCa samples with and without calcium. In the calcium-free hybrids a higher proportion of Q^4 species was observed compared to the calcium-containing hybrids (Fig. 8, Table 3). The Q^4 species increased from 60% to 71% for X_{EC} = 50 and for X_{EC} = 2 from 53% to 66%. This indicates that the incorporation of calcium in the hybrid samples leads to a more polymerised chain-like silica network. Therefore the Ca^{2+} ion interacts with the gelling catalyst HF by lowering its catalytic

activity. The time for gel formation supports this, where the calcium-containing 2ECCa gelled in 60 minutes while the calcium-free 2EC gelled in less than 2.4 minutes. This also suggests that calcium is not incorporated in the silica matrix at this stage and that the calcium is present in the gelling solution.

Bioactivity of the hybridsd in SBF

A major advantage of a hybrid material over a conventional composite is that the surface between the material and the SBF in a hybrid is composed of both organic and inorganic phases, while often in macroscale composites the inorganic phase can be enclosed by the organic phase.[47] Therefore in a hybrid the inorganic bioactive phase is readily available for the mechanisms of HCA formation to take place, while in a macro composite the encompassing organic phase has to resorb first for the inorganic phase to be come in contact with the SBF. Although in some organic polymer systems the SBF solution may diffuse through the organic chains and react with the enclosed inorganic, this however still delays the formation of HCA and aditionally the newly formed HCA may also be enclosed by the organic polymer. The rate of HCA formation in SBF of the inorganic $70SiO_2 30CaO$ (70S30C), hybrid 50EC, 50ECCa and 100ECCa samples were tested by immersion in SBF for periods of up to 72 h. Fig. 9a shows the Ca, P and Si concentrations obtained by performing inductively coupled plasma (ICP) analysis on the SBF solutions after each immersion time point. All the samples containing calcium in their initial composition showed increased levels of calcium in the SBF shortly after immersion, indicating that Ca ions were released almost immediately. Thereafter, the Ca ion concentration in SBF solution decreased as a function of immersion time due to uptake by the samples and HCA formation. Although, the 50EC calcium-free hybrid showed very small changes in Ca ion concentration as immersion time increased. The phosphate content of the SBF decreased as immersion time increased for all samples except 50EC. The decrease is attributed to deposition of phosphate species on the material surface. 50EC (calcium free) is therefore not expected to be bioactive. The most rapid decrease in phosphate was concurrent with rapid uptake of calcium (up to 24 h) after which both phosphate and Ca uptake levelled off, indicating that the newly deposited material was rich in calcium-phosphate (Ca-P). The 70S30C material caused the most rapid phosphate deposition. The 100ECCa hybrid sample had the second steepest decrease in Ca and P while the 50ECCa with higher X_{EC} ratio had the slowest uptake of all the calcium-containing samples. Therefore the uptake of Ca and P were interdependent and higher crosslinking decreased the release rate of Ca from the sample.

All the samples had similar Si release profiles with the highest release rate up until 24 h immersion. Of all the samples the maximum release after 72 h of immersion was 56 μgml^{-1} close to the solutiblity limit for Si under these conditions for the calcium-free sample 50EC while the 100ECCa had the lowest Si release of 38 μgml^{-1}.

Fourier transform infrared (FTIR) spectroscopy was performed on the immersed samples to detect the presence of Ca-P bonds. The Ca-P bending vibration has a distinct double band in the spectra at around 565 and 595 cm^{-1} wavenumbers.[48] Fig. 9b shows the FTIR spectra of the hybrids 50ECCa and 100ECCa. The FTIR confirms that a carbonated calcium phosphate deposited on the 100ECCa hybrid sample within 24 h of immersion. The intensity of the

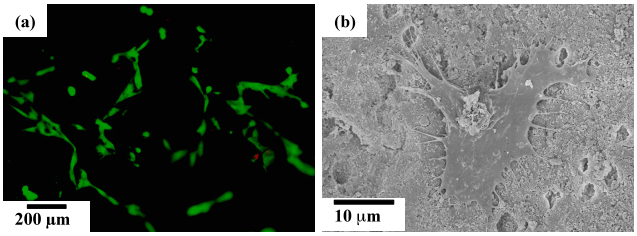

Fig. 10 LIVE/DEAD staining of SaOs-2 cells cultured on 100ECCa hybrid (a) and SEM image (b) of a single cell on the hybrid surface.

bands increased after 72 h immersion, indicating that the layer grew with further immersion. The 50ECCa hybrid however did not show any evidence for the presence of Ca-P after 72 h of immersion in SBF, indicating that no HCA was deposited in 72 h. X-ray diffraction (XRD) was used to confirm whether the deposited Ca-P layer on the sample was a crystalline HCA by comparing the XRD to a standard HA diffraction pattern. Fig. 9c shows the XRD pattern of the 100ECCa sample after 24 h and 72 h immersion, it also includes the pattern of a synthetic HCA (Reference code 00-009-0432). The pattern from 100ECCa after 24 h and 72 h immersion had similar amorphous backgrounds due to the silica matrix and distinct sharp peaks at {210} and {222}. These peaks were identified as being calcium fluoride. Small amounts of calcium fluoride may have formed due to free fluoride ions being present after gelation of the silica by HF. The formation of calcium fluride after soaking in SBF has been reported by Brauer *et. al.* on fluoride containing phosphate glasses.[49] Due to the small quantity of fluoride present, the amount of calcium fluoride must be small and therefore is not expected to affect cell response. Only after 72 h immersion were peaks corresponding to HCA found, indicating that the calcium phosphate that deposited after 24 h immersion (FTIR) was amorphous and had not crystallised until 72 h. Fig. 9d shows an SEM image of the surface of the 100ECCa nanocomposite immersed in SBF for 72 h. The sharp needle-like particles seen in the image were similar to the HCA particles formed on sol-gel glasses.[28]

The SBF tests indicated that calcium was required in the initial composition of the samples for HCA formation. It also showed that by doubling the crosslinking from 100ECCa to 50ECCa the formation of the HCA was hindered. This was due to the more compact structure of the higher crosslinked hybrid which gave rise to slower dissolution of calcium.

Cell attachment and LIVE/DEAD assay

The synthesis of the hybrid involved the use of toxic reagents, especially TEOS, GPTMS and DMSO. Some of these may have remained in the hybrid after the drying process, therefore

the toxicity of this material was tested with SaOs-2 cells. Fig. 10a shows a representative image of cells stained with the LIVE/DEAD cell viability assay following culture on the hybrid for 4 days. The assay demonstrated that there were many live cells (green) and very few dead cells (red) indicating that the hybrid was not cytotoxic and did not induce cell death. Fig. 10b shows a SEM image of a cell attaching on the hybrid surface after 4 days of culture. SEM revealed that the cells attached and spread on the hybrid surface with large and multiple adhesion areas indicating strong attachment to the material.

Conclusions

Poly(γ-glutamic acid)/ silica class II hybrids were successfully synthesised with covalent bonding between the organic and inorganic phases, which was proven by the presence of both T^n and Q^n species detected by ^{29}Si NMR. This was achieved by incorportating functionalised poly(γ-glutamic acid) into a silica sol. With increasing coupling agent (GPTMS) higher proportions of T^n species were observed, which was also found to increase inorganic/organic interaction, improving the integration of the two materials. The amount of the aprotic solvent (DMSO) in the hybrid sol had a large influence on the final structure of the hybrid due to the high hydrogen bonding ability and templating affect of the solvent. It was determined that the solute concentration, S_{ED} ratio, should be higher than 0.23 for optimum hybrid nanostructure, where the organic and inorganic had nanoscale domains and were continuous through out the hybrid.

The incoporation of calcium eliminated mesopores in the hybrid and induced HCA formation. An SBF study showed that HCA deposited on the hybrids and increased crosslinking decreased the rate of HCA formation. The hybrid with an X_{EC} ratio of 100 formed well developed HCA after just 3 days of immersion. The hybrid material was not toxic to the osteosarcoma cell line SaOs-2 and the cells were able to spreading and form large and multiple adhesions to the sample surface. Porous versions of these hybrids would therefore have potential as scaffolds for bone regeneration applications.

Experimental

The two pot reaction procedure for the synthesis of the class II 40 wt% γ-PGA with 60 wt% bioactive calcium silicate (70 mol% SiO_2, 30 mol% CaO) is described below. The hybrid 50ECCa was produced with glutamic acid:GPTMS ratio of 50:1 and S_{ED} ratio of 0.09. The γ-PGA was purchased in the free acid powder form from Natto Biosciences (Quebec, Canada) with 95 wt% polymer and 5 wt% water. All other materials were purchased from Sigma-Aldrich.

Reaction of γ-PGA and GPTMS

Poly(γ-glutamic acid) and GPTMS (99.8%) were first reacted in DMSO (98.5) under a nitrogen atmosphere. 45 ml of 98.5% DMSO and 5 g of γ-PGA in a flask with N_2 flowing over the solvent was heated to 80°C while mixing with a magnetic stirrer. To the dissolved polymer solution 0.18 g of 99.8% GPTMS dissolved in 5 ml DMSO was added drop-wise and the reaction was allowed to proceed for 8 h. After the completion of the reaction rotary vacuum evaporation at 80°C was performed to evaporate 65 vol% of DMSO (32.5 ml) from the reaction solution which gives an S_{ED} (wt/wt) ratio of 0.26.

Reaction of organic and inorganic

After the evaporation of required amount of DMSO; 4.7 g of $CaCl_2$ dissolved in 9.4 ml of deionised water was added and was allowed to mix for 5 minutes.

In a separate beaker 9.4 ml of deionised water, 6.5 ml of 1N hydrochloric acid and 20.5 ml of tetraethyoxysilane (TEOS) were dissolved in order and left to react for 1 h. The reacted inorganic precursor solution was then added to the functionalised polymer/$CaCl_2$ solution and left mixing for 1 h. A 10 ml aliquot of this solution was poured into poly (fluoro alkoxy) (PFA) moulds and gelled with 0.6 ml of 5 vol% hydrofluoric acid (HF). Once gelled, they were immediately sealed and transferred to a heated oven. The sealed samples were aged at 60 °C for 3 days followed by opening the moulds to dry at 60 °C until completely dry.

Hybrids with X_{EC} ratios of 2 (2ECCa), 10 (10ECCa) and 100 (100ECCa) were also produced using the same method mentioned above.

Characterisation of hybrids

Solid state NMR

^{29}Si MAS NMR spectra of the hybrid samples were collected on a Varian InfinityPlus 300 spectrometer (7.05 T) operating at 59.62 MHz, using a Varian 7.5 mm probe spinning at 4 kHz. A 4.5 µs pulse (~45°) was applied with a 30 s recycle delay. ^{29}Si NMR spectra were referenced to TMS at 0 ppm.

Electron microscopy studies

A LEO 1525 scanning electron microscope (SEM) equipped with a GEMINI field emission column was used to image the hybrid fracture surface. All samples were ground to powder in liquid nitrogen, mounted on sticky carbon tape and sputter coated with chromium to a maximum thickness of 15 nm before imaging. Images were collected on the in-lens secondary electron detector with an operating voltage of 5 kV and a working distance of 5-8 mm.

A JEOL 2010 TEM equipped with a LaB_6 filament was used for TEM studies. An operating voltage of 200 kV was used on powder samples deposited on holey carbon TEM grids.

Pore measurement

Nitrogen adsorption (Quantachrome AS6) and high pressure mercury porosimetry (Quantachrome Poremaster 33) were used to determine the meso and macro pore network of the hybrid samples. The BET[50] and BJH[51] models were applied to the adsorption and desorption branches of the nitrogen sorption isotherm to obtain surface area and pore size distribution, respectively.

Bioactivity in SBF

Bioactivity of the hybrid samples were tested by immersion in SBF. SBF solution has a similar concentration of positive ions as in human blood plasma.[52] Rectangular monolithic samples

of approximate dimensions 5 x 5 x 3 mm^3 were used. Samples immersed in SBF (pH 7.4) for 8, 24, 72 h were agitated at a constant rotation speed of 120 rpm in an orbital shaker at 37°C. The pH of the solution before and after the tests was measured. The Ca, Si and P ion concentrations in the filtered solutions were also measured using inductively coupled plasma optical emission spectroscopy (ICP-OES). FTIR, XRD and SEM measurements were performed on the samples to determine the formation of an HCA layer.

Cytotoxicity

The osteosarcoma cell line SaOs-2 was used for a cell culture study on the 100ECCa hybrid. Samples were cut to 5 × 5 ×3 mm^3 pieces, sterilised by autoclaving and incubated in culture medium supplemented with 50 μg/ml penicillin, 50 μg/ml streptomycin, 2.5 μg/ml amphotericin B at 37 °C for 48 h (preconditioning). Following preconditioning, the hybrids were seeded with 100,000 cells. and were cultured at 37 °C 5% CO_2 for a period of 4 days.

Cell viability/cytotoxicity was assessed using the LIVE/DEAD assay (Molecular Probes, UK), which was performed according to the manufacturer's instructions. Stained samples were examined under an Olympus BX-URA2 fluorescence microscope and images were captured using a Zeiss Axiocam digital camera and analysed using KS-300 software (Imaging Associates). SEM was used to assess cell attachment and morphology. Cells were fixed in 2.5% (w/v) glutaraldehyde for 40 min at 4 °C followed by dehydration through a series of increasing concentrations of ethanol and a final incubation in hexamethyldisilazane (HMDS). Samples were sputter coated with gold and viewed on a scanning electron microscope (Gemini 1525 FEGSEM).

Acknowlegements

The authors wish to thank the following funding bodies: EPSRC (especially EP/E057098/1 and EP/051669/1), ERC FP7 grant "Naturale" (MMS) and the Philip Leverhulme Prize (JRJ). JRJ was a Royal Academy of Engineering and EPSRC Research Fellow.

Notes

[a] *Department of Materials, Imperial College London, South Kensington, UK. Fax: 20 7594 6757; Tel: 20 7594 6749.*
E-mail: julian.r.jones@imperial.ac.uk
[b] *Department of Physics, University of Warwick, Coventry, UK.*
[c] *Institute of Biomedical Engineering, Imperial College London, UK*
[d] *Faculty of Medicine, National Heart & Lung Institute, Imperial College London, UK.*
[e] *Dental Physical Science Unit, Queen Mary London, UK.*

References

1. A. A. Jahangir, M. R. Nunley, S. Mehta, A. Sharan and W. H. P. Fellows, in *AAOS Now*, 2008, p. 5.
2. C. R. Perry, *Clin. Orthop. Rel. Res.*, 1999, 71-86.
3. C. Laurencin, Y. Khan and S. F. El-Amin, *Expert Rev. Med. Devices*, 2006, **3**, 49-57.
4. H. Oonishi, S. Kushitani, E. Yasukawa, H. Iwaki, L. L. Hench, J. Wilson, E. I. Tsuji and T. Sugihara, *Clin. Orthop. Rel. Res.*, 1997, 316-325.
5. J.-Y. Rho, L. Kuhn-Spearing and P. Zioupos, *Med. Eng. Phys.*, 1998, **20**, 92-102.
6. C. Z. Liu and J. T. Czernuszka, *Mater. Sci. Technol.*, 2007, **23**, 379-391.
7. J. R. Jones, L. M. Ehrenfried and L. L. Hench, *Biomaterials*, 2006, **27**, 964-973.
8. J. R. Jones, P. D. Lee and L. L. Hench, *Phil Trans Roy Soc A*, 2006, **364**, 263-281.
9. R. Langer, *MRS Bull.*, 2006, **31**, 477-485.
10. L. L. Hench and J. M. Polak, *Science*, 2002, **295**, 1014-1017.
11. L. L. Hench and J. R. Jones, *Biomaterials, Artificial Organs and Tissue Engineering*, Woodhead Publishing Limited, Abington, 2005.
12. C. E. Holy, J. A. Fialkov, J. E. Davies and M. S. Shoichet, *J. Biomed. Mater. Res. A*, 2003, **65A**, 447-453.
13. X. Liu and P. X. Ma, *Ann. Biomed. Eng.*, 2004, **32**, 477-486.
14. E. S. Place, J. S. George, C. K. Williams and M. M. Stevens, *Chem. Soc. Rev.*, 2009, **38**, 1139-1151.
15. E. S. Place, N. D. Evans and M. M. Stevens, *Nature Mater.*, 2009, **8**, 457-470.
16. Z. Xiong, Y. N. Yan, S. G. Wang, R. J. Zhang and C. Zhang, *Scripta Mater.*, 2002, **46**, 771-776.
17. J. Blaker and A. Boccaccini, *Expert Rev. Med. Devices*, 2005, **2**, 303-317.
18. R. Tang and Y. Cai, *J. Mater. Chem.*, 2008, **18**, 3775-3787.
19. S. Misra, D. Mohn, T. J. Brunner, W. J. Stark, S. E. Philip, I. Roy, S. V., J. C. Knowles and A. R. Boccaccini, *Biomaterials*, 2008, **29**, 1750-1761.
20. O. Mahony and J. R. Jones, *Nanomedicine*, 2008, **3**, 233-245.
21. M. M. Stevens, *Materials Today*, 2008, **11**, 18-25.
22. J. R. Jones, *J. Eur. Ceram. Soc.*, 2009, **29**, 1275-1281.
23. P. Saravanapavan, *J Biomed. Mater. Res.*, 2001, **54**, 608-618.
24. L. L. Hench, *Curr. Opin. Solid State Mater. Sci.*, 1997, **2**, 604-610.
25. S. K. Young, G. C. Gemeinhardt, J. W. Sherman, R. F. Storey, K. A. Mauritz, D. A. Schiraldi, A. Polyakova, A. Hiltner and E. Baer, *Polymer*, 2002, **43**, 6101-6114.
26. D. Tian, P. Dubois and R. Jerome, *J. Polym. Chem. A*, 1997, **35**, 2295-2309.
27. T. Ogoshi and Y. Chujo, *J. Mater. Chem.*, 2005, **15**, 315-322.
28. M. Vallet-Regi and D. Arcos, *Current Nanoscience*, 2006, **2**, 179-189.
29. M. M. Pereira, J. R. Jones, R. L. Orefice and L. L. Hench, *J. Mater. Sci. Mater. Med.*, 2005, **16**, 1045-1050.
30. L. Ren, K. Tsuru, S. Hayakawa and A. Osaka, *Biomaterials*, 2002, **23**, 4765-4773.
31. P. Judeinstein, P. W. Oliveira, H. Krug and H. Schmidt, *Chem. Phys. Lett.*, 1994, **220**, 35-39.
32. B. M. Novak, *Adv. Mater.*, 1993, **5**, 422-433.
33. N. Husing, U. Schubert, K. Misof and P. Fratzl, *Chem. Mater.*, 1998, **10**, 3024-3032.
34. L. Ren, K. Tsuru, S. Hayakawa and A. Osaka, *J. Sol-gel Sci. Technol.*, 2001, **21**, 115-121.

35. K. Fan, D. Gonzales and M. Sevoian, *J. Environ. Polym. Degrad.*, 1996, **4**, 253-260.
36. A. Sugino, T. Myiyazaki and C. Ohtsuki, *Key Eng. Mater.*, 2007, **330-332**, 683-686.
37. G. K. Hunter and H. A. Goldberg, *Biochemical Journal*, 1994, **302**, 175-179.
38. P. J. Gorski, *Calcif. Tissue Int.*, 1992, **50**, 391-396.
39. S. Lin, C. Ionescu, K. J. Pike, M. E. Smith and J. R. Jones, *J. Mater. Chem.*, 2009, **19**, 1276-1282.
40. C. J. Brinker, *J. Non-Cryst. Solids*, 1988, **100**, 31-50.
41. K. Sing, D. Everett, R. Haul, L. Moscou, R. Pierotti, J. Rouquerol and T. Siemieniewska, *Pure Appl. Chem.*, 1985, **57**, 603-619.
42. Gregg SJ and Sing KSW, *Adsorption, Surface Area and Porosity*, Academic Press, 1967.
43. I. D. Xynos, A. J. Edgar, L. D. Buttery, L. L. Hench and J. M. Polak, *J. Biomed. Mater. Res.*, 2001, **55**, 151-157.
44. K. J. D. Mackenzie and M. E. Smith, *Multinuclear solid state NMR of inorganic materials*, Pergamon Press, Oxford, 2002.
45. D. Massiot, F. Fayon, M. Capron, B. Alonso, J. O. Durand, B. Bujoli, Z. Gan and G. Hoatson, *Magn. Reson. Chem.*, 2002, **40**, 70-76.
46. C. J. Brinker and G. W. Scherer, *Sol-gel science: The physics and chemistry of sol-gel processing*, Academic Press, San Diego, 1990.
47. M. Navarro, *Ordered Polymeric Nanostructures at Surfaces*, 2006, **200**, 209-231.
48. B. Fowler, *Inorg Chem.*, 1974, **13**, 194-207.
49. D. S. Brauer, N. Karpukhina, M. D. O'Donnell, R. V. Law and R. G. Hill, *Acta Biomater.* , 2010, **doi:10.1016/j.actbio.2010.01.043**.
50. S. Brunauer, P. H. Emmett and E. Teller, *JACS*, 1938, **60**, 309-319.
51. P. E. Barrett, G. L. Joyner and P. P. Halenda, *JACS*, 1951, **41**, 373-380.
52. T. Kokubo, H. Kushitani, S. Sakka, T. Kitsugi and T. Yamamuro, *J Biomed. Mater. Res.*, 1990, **24**, 721-734.

Figure captions

Fig 1. Schematic of the two pot reaction for the hybrid synthesis. Poly(γ-glutamic acid) and glycidoxypropyl trimethoxysilane (GPTMS) are first reacted to get silane coupling on the polymer. Then calcium is added as $CaCl_2$ dissolved in water. In the second pot the TEOS is hydrolysed in acidic conditions. The two pots are mixed together resulting in the hybrid precursor sol.

Fig 2. The T^n and Q^n Si-O bridging configurations that could occur in the hybrid material as determined by ^{29}Si NMR.

Fig. 3. Flow chart showing the reaction and processing steps involved in the synthesis of the hybrid material.

Fig. 4. SEM images of the fracture surface of hybrids containing 40 wt% organic, 60 wt% inorganic and γ-PGA:DMSO ratio (S_{ED}) of 0.09 (a,b), 0.23 (c,d), 0.26 (e,f) and 0.45 (g,h).

Fig. 5. (a) Nitrogen sorption isotherms of hybrids with various γ-PGA:DMSO ratios (S_{ED}) and (b) pore size distributions of the same materials obtained from the N_2 desorption isotherm and mercury porosimetry.

Fig. 6. SEM and TEM images showing the influence of calcium on the nanostructure of the hybrids. SEM image of hybrid without calcium (a), with calcium (b,c) and TEM image of hybrid with calcium (d).

Fig. 7. TEM image and N_2 sorption isotherm of the hybrid before (a,c) and after extraction of the polymer (b,d).

Fig. 8. ^{29}Si MAS NMR spectra of hybrids with increasing amounts of crosslinker (a) and with and without calcium (b).

Fig, 9. SBF testing of $70SiO_2 30CaO$, 50EC, 50ECCa and 100ECCa. (a) ICP spectra of the SBF solutions removed at 1, 24 and 72 h. (b) FTIR spectra of 100ECCa after 1, 24 and 72 h soaking and of 72 h of soaked 50ECCa. (c) XRD spectra of 100ECCa hybrid sample after 24 and 72 h of soaking and of synthetic HCA (Reference code 00-009-0432). (d) SEM image of the 100ECCa sample after soaking for 72 h showing the needle like HCA particles formed on the hybrid.

Fig. 10. LIVE/DEAD staining of SaOs-2 cells cultured on 100ECCa hybrid (a) and SEM image (b) of a single cell on the hybrid surface.

Tables

Table 1. Summary of the influence of the three processing parameters during coupling reaction on the condensation of the GPTMS trimethoxy silicate groups.

Table 2. Summary of the meso and macro porosity of the hybrids with γ-PGA:DMSO ratio (S_{ED}) of 0.09, 0.23, 0.26 and 0.45.

Table 3. Chemical shifts and relative proportions of T^n and Q^n species in the hybrids with different proportions of coupling and with and without calcium.

δ and I represent the ^{29}Si chemical shift and relative intensity, respectively. Errors associated with measurements are δ ± 2 ppm and Integral ±2%.